

# We are IntechOpen, the world's leading publisher of Open Access books Built by scientists, for scientists

6,900

Open access books available

186,000

International authors and editors

200M

Downloads

Our authors are among the

154

Countries delivered to

TOP 1%

most cited scientists

12.2%

Contributors from top 500 universities



WEB OF SCIENCE™

Selection of our books indexed in the Book Citation Index  
in Web of Science™ Core Collection (BKCI)

Interested in publishing with us?  
Contact [book.department@intechopen.com](mailto:book.department@intechopen.com)

Numbers displayed above are based on latest data collected.  
For more information visit [www.intechopen.com](http://www.intechopen.com)



# Stability, Dynamic and Aeroelastic Optimization of Functionally Graded Composite Structures

Karam Maalawi

Additional information is available at the end of the chapter

<http://dx.doi.org/10.5772/45878>

## 1. Introduction

Numerous applications of numerical optimization to various structural design problems have been addressed in the literature. A comprehensive survey on this issue was given in [1], presenting a historical review and demonstrating the future needs to assimilate this technology into the practicing design environment. Different approaches were applied successfully by several investigators for treating stress, displacement, buckling and frequency optimization problems. In general, design optimization seeks the best values of a set of  $n$  design variables represented by the vector,  $\underline{X}_{n \times 1}$ , to achieve, within certain  $m$  constraints,  $\underline{G}_{m \times 1}(\underline{X})$ , its goal of optimality defined by a set of  $k$  objective functions,  $\underline{F}_{k \times 1}(\underline{X})$ , for specified environmental conditions (see Figure 1). Mathematically, design optimization may be cast in the following standard form: Find the design variables  $\underline{X}_{n \times 1}$  that minimize

$$F(\underline{X}) = \sum_{i=1}^k W_{fi} F_i(\underline{X}) \quad (1a)$$

subject to

$$G_j(\underline{X}) \leq 0, \quad j=1,2,\dots,I \quad (1b)$$

$$G_j(\underline{X}) = 0, \quad j=I+1,I+2,\dots,m \quad (1c)$$

$$0 \leq W_{fi} \leq 1$$

$$\sum_{i=1}^k W_{fi} = 1 \quad (1d)$$

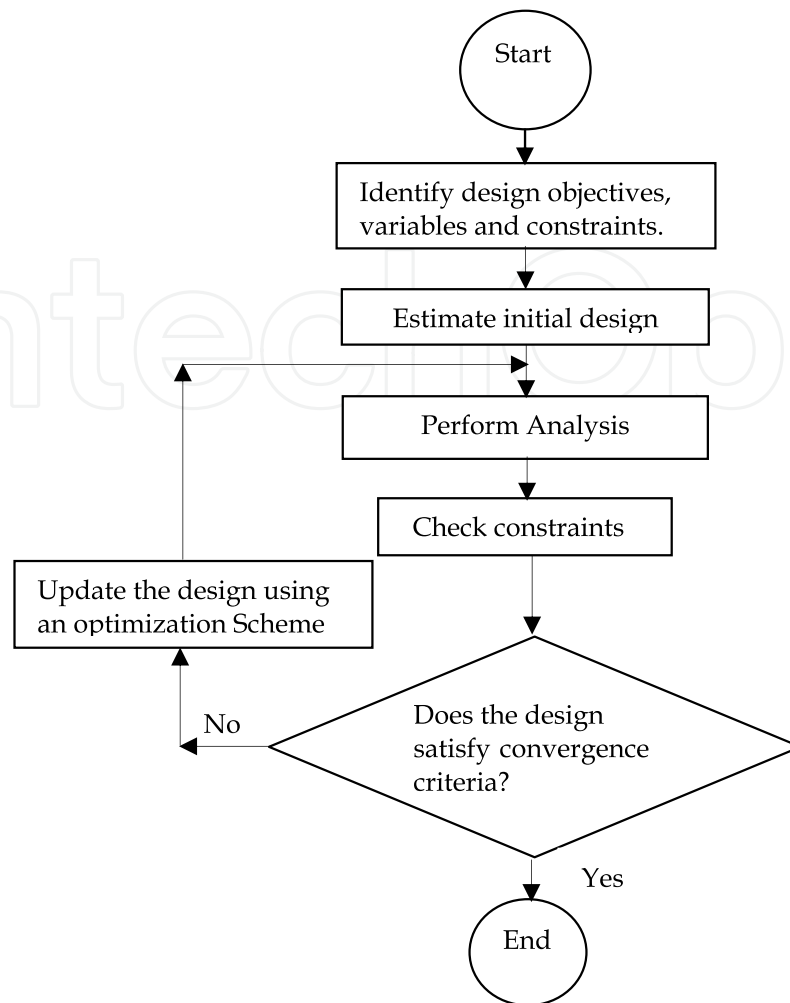


**Figure 1.** Design optimization process

The weighting factors  $W_{fi}$  measure the relative importance of the individual objectives with respect to the overall design goal. Several computer program packages are available now for solving a variety of design optimization models. Advanced procedures are carried out by using large-scale, general purpose, finite element-based multidisciplinary computer programs [2], such as *ASTROS*, *MSC/NASTRAN* and *ANSYS*. The *MATLAB* optimization toolbox is also a powerful tool that includes many routines for different types of optimization encompassing both unconstrained and constrained minimization algorithms [3]. Design optimization of sophisticated structural systems involves many objectives, constraints and variables. Therefore, creation of a detailed optimization model incorporating, simultaneously, all the relevant design features is virtually impossible. Researchers and engineers rely on simplified models which provide a fairly accurate approximation of the real structure behaviour. This chapter presents some of the underlying concepts of applying optimization theory for enhancing the stability, dynamic and aeroelastic performance of functionally graded material (*FGM*) structural members. Such concept of *FGM*, in which the properties vary spatially within a structure, was originated in Japan in 1984 during the space project, in the form of proposed thermal barrier material

capable of withstanding high temperature gradients. *FGMs* may be defined as advanced composite materials that fabricated to have graded variation of the relative volume fractions of the constituent materials. Commonly, these materials are made from particulate composites where the volume fraction of particles varies in one direction, as shown in Figure 2, or several directions for certain applications. *FGMs* may also be developed using fiber reinforced layers with a volume fractions of fibers changing, rather than constant, producing grading of the material with favorable properties.

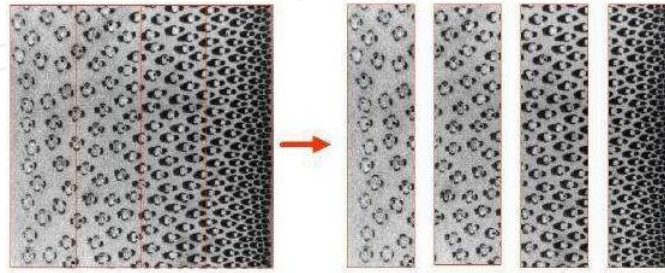


**Figure 2.** The concept of material grading

Table 1 summarizes the mathematical formulas for determining the equivalent mechanical and physical properties for known type and volume fractions of the fiber and matrix materials [4]. The factor  $\xi$  is called the reinforcing efficiency and can be determined experimentally for specified types of fiber and matrix materials. Experimental results fall within a band of  $1 < \xi < 2$ . Usually,  $\xi$  is taken as 100% for theoretical analysis procedures, especially in case of glass and carbon composites. The 1 and 2 subscripts denote the principal directions of an orthotropic lamina, defined as follows: direction (1): principal fiber direction, also called fiber longitudinal direction; direction (2): In-plane direction perpendicular to fibers, transversal direction.

Property	Mathematical formula*
Young's modulus in direction (1) $E_{11}$	$E_m V_m + E_{1f} V_f$
Young's modulus in direction (2) $E_{22}$	$E_m (1 + \xi \eta V_f) / (1 - \eta V_f); \quad \eta = (E_{2f} - E_m) / (E_{2f} + \xi E_m)$
Shear modulus $G_{12}$	$G_m (1 + \xi \eta V_f) / (1 - \eta V_f); \quad \eta = (G_{12f} - G_m) / (G_{12f} + \xi G_m)$
Poisson's ratio $\nu_{12}$	$\nu_m V_m + \nu_{12f} V_f$
Mass density $\rho$	$\rho_m V_m + \rho_f V_f$
*Subscripts "m" and "f" refer to properties of matrix and fiber materials, respectively. Assuming no voids are present, then $V_m + V_f = 1$ .	

**Table 1.** Halpin-Tsai semi-empirical relations for calculating composite properties [4].

An excellent review paper dealing with the basic knowledge and various aspects on the use of FGMs and their wide applications was given in [5]. It was shown that FGMs can be promising in several applications such as, spacecraft heat shields, high performance structural elements and critical engine components. A few studies have addressed the dynamics and stability of FGM structures. Closed-form expressions for calculating the natural frequencies of an axially graded beam were derived in [6]. The modulus of elasticity was taken as a polynomial of the axial coordinate along the beam's length, and an inverse problem was solved to find the stiffness and mass distributions so that the chosen polynomial serve as an exact mode shape. Another work [7] considered stability of FGM-structures and derived closed form solution for the mode shape and the buckling load of an axially graded cantilevered column. A semi-inverse method was employed to obtain the spatial distribution of the elastic modulus in the axial direction. In reference [8], the buckling of simply supported three-layer circular cylindrical shell under axial compressive load was considered. The middle layer sandwiched with two isotropic layers was made of an isotropic FGM whose Young's modulus varies parabolically in the thickness direction. Classical shell theory was implemented under the assumption of very small thickness/radius and very large length/radius ratios. Numerical results showed that the buckling load increases with an increase in the average value of Young's modulus of the middle layer. In the field of structural optimization, reference [9] considered frequency optimization of a cantilevered plate with variable volume fraction according to simple power-laws. Genetic algorithms was implemented to find the optimum values of the power exponents, which maximize the natural frequencies, and concluded that the volume fraction needs to be varied in the longitudinal direction of the plate rather than in the thickness direction. A direct method was proposed in [10] to optimize the natural frequencies of functionally graded beam with variable volume fraction of the constituent materials in the beam's length and height directions. A piecewise bi-cubic interpolation of volume fraction values specified at a finite number of grid points was used, and a genetic algorithm code was applied to find the needed optimum designs. It is the main aim of this chapter to present some fundamental issues concerning design optimization of different types of functionally graded composite structures. Practical realistic optimization models using different strategies for enhancing stability, structural dynamics, and aeroelastic performance are presented and discussed. Design variables represent material type, structure geometry as well as cross sectional parameters. The mathematical formulation is based on dimensionless quantities; therefore the analysis can be valid for different configurations and sizes. Such normalization has led to a naturally scaled optimization models, which is favorable for most optimization techniques. Case studies concerning optimization of FGM composite structures include buckling of flexible columns, stability of thin-walled cylinders subject to external pressure, frequency optimization of FGM bars in axial motion, and critical velocity maximization in pipe flow as a measure of raising the stability boundary. The use of the concept of material grading for enhancing the aeroelastic stability of composite wings have been also addressed. Several design charts that are useful for direct

determination of the optimal values of the design variables are introduced. In all, the given mathematical models can be regarded as useful design tools which may save designers from having to choose the values of some of their variables arbitrarily.

## 2. Buckling optimization of elastic columns

The consideration of buckling stability of elastic columns can be crucial factor in designing efficient structural components. In references [11, 12], optimization models of the strongest columns were developed for maximizing the critical buckling load under equality mass constraint. Emphasizes were given to thin-walled tubular sections, which are more economical than solid sections in resisting compressive loads. The given formulation considered columns made of uniform segments with different material properties, cross-sectional parameters and length, as shown in Figure 3. The simplest problem of equilibrium of a column compressed by an axial force,  $P$ , was first formulated and solved by the great mathematician L. Euler in the middle of the eighteenth century. The associated 4th-order governing differential equation in dimensionless form:

$$\hat{w}'''' + P_k^2 \hat{w} = 0, \quad P_k = \sqrt{\hat{P} / \hat{E}_k \hat{I}_k}, \quad k=1, 2, \dots, N_s \quad (2)$$

where ( )' means differentiation with respect to the dimensionless coordinate  $\hat{x}$  and  $N_s$  is the total number of segments. The various dimensionless quantities denoted by ( ^ ) are defined in Table 2. Equation (2) must be satisfied in the interval  $0 \leq \bar{x} \leq L_k$ , where  $\bar{x} = \hat{x} - \hat{x}_k$ . Its general solution is:

$$\hat{w}(\bar{x}) = a_1 \sin P_k \bar{x} + a_2 \cos P_k \bar{x} + a_3 \bar{x} + a_4 \quad (3)$$

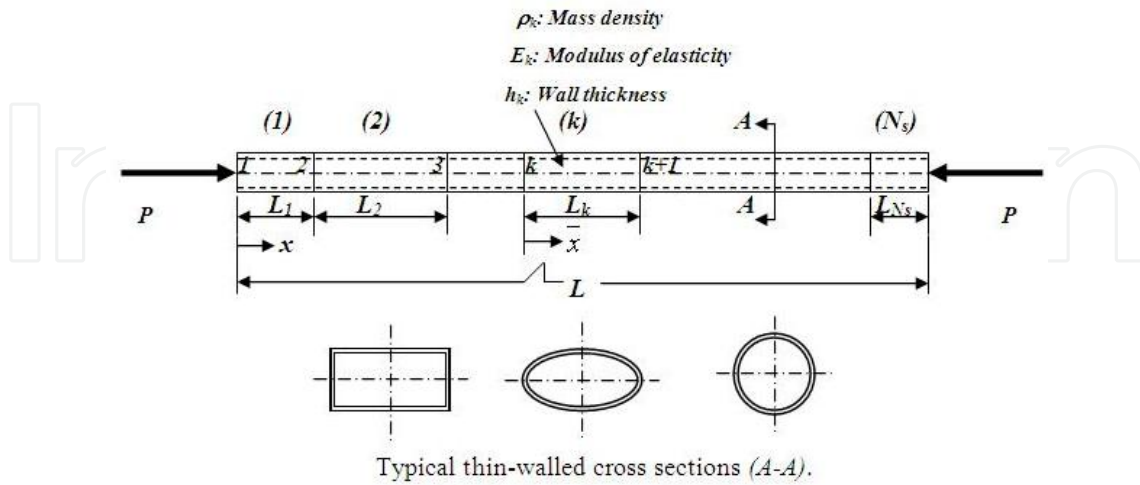


**Figure 3.** General configuration of a piecewise axially graded thin-walled column

The coefficients  $a_i$ 's in Equation (3) can be expressed in terms of the state variables at both nodes of the  $K$ th segment, which results in the following matrix relation:

$$\begin{Bmatrix} \hat{w}_{k+1} \\ \phi_{k+1} \\ \hat{M}_{k+1} \\ \hat{F}_{k+1} \end{Bmatrix} = \begin{bmatrix} 1 & \frac{-S_k}{P_k} & \frac{-(1-C_k)}{\hat{P}} & (\frac{S_k}{\hat{P}P_k} - \frac{\hat{L}_k}{\hat{P}}) \\ 0 & C_k & \frac{P_k S_k}{\hat{P}} & \frac{(1-C_k)}{\hat{P}} \\ 0 & \frac{-\hat{P}S_k}{P_k} & C_k & \frac{S_k}{P_k} \\ 0 & 0 & 0 & 1 \end{bmatrix} \begin{Bmatrix} \hat{w}_k \\ \phi_k \\ \hat{M}_k \\ \hat{F}_k \end{Bmatrix} \quad (4)$$

where  $S_k = \sin P_k L_k$  and  $C_k = \cos P_k L_k$ . Applying Equation (4) successively to all the segments composing the column and taking the products of all the resulting matrices, the state variables at both ends of the column can be related to each other through an overall transfer matrix. Therefore, by the application of the appropriate boundary conditions and consideration of the non-trivial solution, the associated characteristic equation for determining the critical buckling load can be accurately obtained. The exact buckling analysis outlined above can be coupled with a standard nonlinear mathematical programming algorithm for the search of columns designs with the largest possible resistance against buckling. It is important to bear in mind that design optimization is only as meaningful as its core structural analysis model. Any deficiencies therein will certainly be reflected in the optimization process.

Quantity	Non-dimensionalization*
Axial coordinate	$\hat{x} = x / L$
Length of $K$ th segment	$\hat{L}_k = L_k / L$
Transverse deflection	$\hat{w} = w / L$
Wall thickness	$\hat{h}_k = h_k / h$
Second moment of area	$\hat{I}_k = I_k / I \quad (= \hat{h}_k^3)$
Modulus of elasticity	$\hat{E}_k = E_k / E$
Bending moment	$\hat{M} = M * (L / EI)$
Shearing force	$\hat{F} = F * (L^2 / EI)$
Axial force	$\hat{P} = P * (L^2 / EI)$
Mass density	$\hat{\rho}_k = \rho_k / \rho$
Total structural mass	$\hat{M}_s = \sum_{k=1}^{N_s} \hat{\rho}_k \hat{h}_k \hat{L}_k$
*Baseline design parameters: $L$ =total column's length, $h$ =wall thickness, $I$ = second moment of area, $E$ =modulus of elasticity $= (E_f + E_m)/2$ , $\rho$ =mass density $= (\rho_f + \rho_m)/2$ .	

**Table 2.** Definition of dimensionless quantities



Therefore, the strongest column design problem may be cast in the following:

Maximize

$$\hat{P}_{cr}$$

Subject to

$$\begin{aligned} \hat{M}_s &= 1 \\ \sum_{k=1}^{N_s} \hat{L}_k &= 1 \end{aligned} \quad (5)$$

Side constraints are always present by imposing lower and upper limits on the design variables to avoid having odd-shaped unrealistic column design in the final optimum solutions. Reference [12] presented optimum patterns for cases of simply supported and cantilevered FGM columns constructed from unidirectional fibrous composites with properties given in Table 3. The case of a symmetrical simply supported (S.S.) column made of E-glass/epoxy and constructed from different number of segments is depicted in Figure 4. For the case of 6-segments, the optimum zone of the dimensionless critical buckling load augmented with the mass equality constraint was determined and found to be well behaved in the selected  $(V_A - L)_3$  design space. Referring to Figure 5, three distinct regions can be observed: two empty regions to the left and right violating the mass equality constraint and the middle feasible region containing the global optimum solution. It is also seen that the optimal feasible domain is bounded from left and right by two heavy zigzagged lines owing to the fact that many contours are stuck to these borderlines and are not allowed to penetrate them for not violating the imposed mass constraint. The final optimum design point was found to be  $(V_A, \hat{L})_{k=1,2,3} = (0.095, 0.0875), (0.38125, 0.140625), (0.69177, 0.271875)$  where  $(P_{cr})_{max} = 11.649375$ . This represents an optimization gain of about 18.0% relative to the baseline value ( $\pi^2$ ). Other types of materials were also addressed in [12] including, carbon/epoxy, S-glass/epoxy, E-glass/Vinyl-ester and S-glass/Vinyl-ester. In all cases the

Composite material	material (A) = Fibers		material (B) = matrix	
	$\rho_A(g/cm^3)$	$E_A (GPa)$	$\rho_B(g/cm^3)$	$E_B(GPa)$
E-glass/epoxy	2.54	73.0	1.27	4.3
S-glass/epoxy	2.49	86.0		
Carbon/epoxy	1.81	235.0		
E-glass/Vinylester	2.54	73.0	1.15	3.5
S-glass/Vinylester	2.49	86.0		

**Table 3.** Material properties of selected fiber-reinforced composites [12]



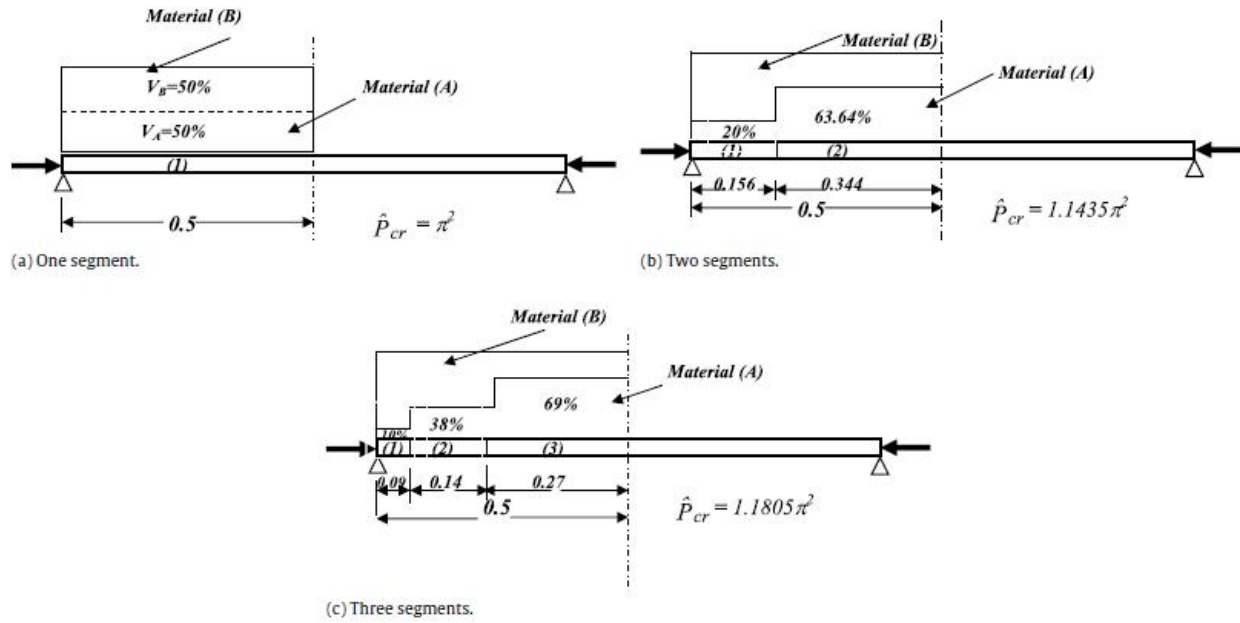


**Figure 4.** Optimum simply supported columns with piecewise axial material grading

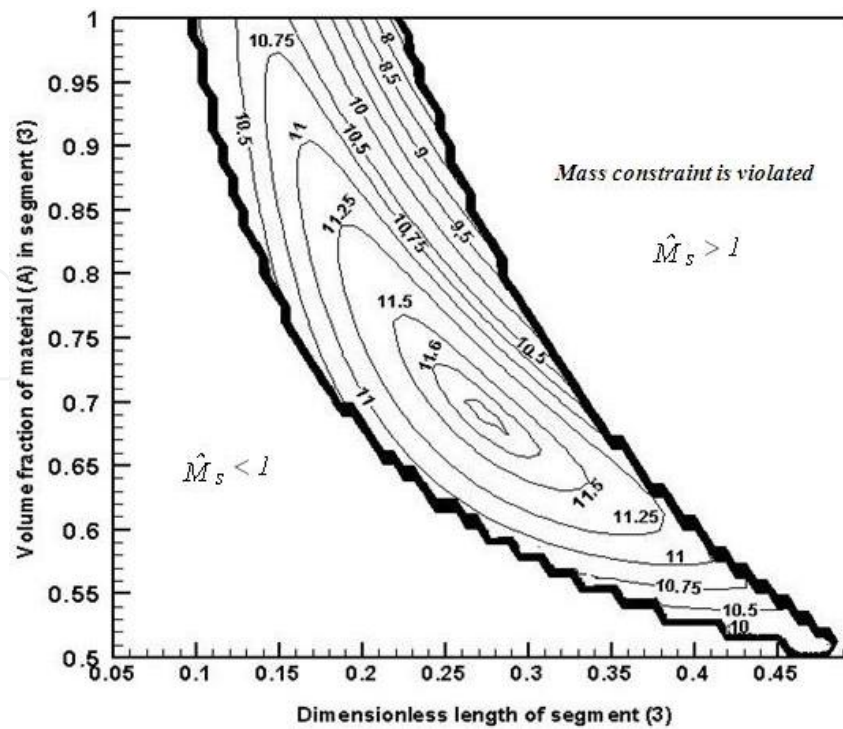


**Figure 5.** Optimum zone for a symmetrical 6-segment S.S. columns made of E-glass/epoxy composites.

buckling load was found to be very sensitive to variation in the segment length. Investigators who use approximate methods, such as finite elements, have not recognized that the length of each element can be taken as a main optimization variable in addition to the cross-sectional properties. The increase in the number of segments would, naturally, result in higher values of the dimensionless critical buckling load. However, care ought to be taken for the corresponding increase in cost due to the resulting complications in the associated assembling and manufacturing procedures.

Other cases of cantilevered columns were also investigated. The associated boundary conditions are: at  $\hat{x}=0$   $\hat{w}=\varphi=0$ , and at  $\hat{x}=1.0$   $\hat{M}=\hat{F}=0$ . Figure 6 shows the attained optimal solutions for cantilevered columns made of unidirectional E-glass/epoxy composites and constructed from different number of segments ( $N_s$ ). For a three-segment column, the global optimal solution was found to be  $(P_{cr})_{max}=2.90938$  occurring at the design point  $(V_A, L_k)_{k=1,2,3} = (0.70, 0.514), (0.4125, 0.2785), (0.122, 0.2075)$ . This means that the strongest column made of only three segments can withstand a buckling load 18% higher than that with uniform mass and stiffness distributions, which represents a truly optimized column design. In fact, the exact buckling load can be obtained for any number of segments, type of cross section and type of boundary conditions. The given multi-segment model has the advantageous of achieving global optimality for the strongest columns shape that can be manufactured economically from any arbitrary number of segments. Sensitivity of the design variables on the buckling load should be included in a more general formulation.

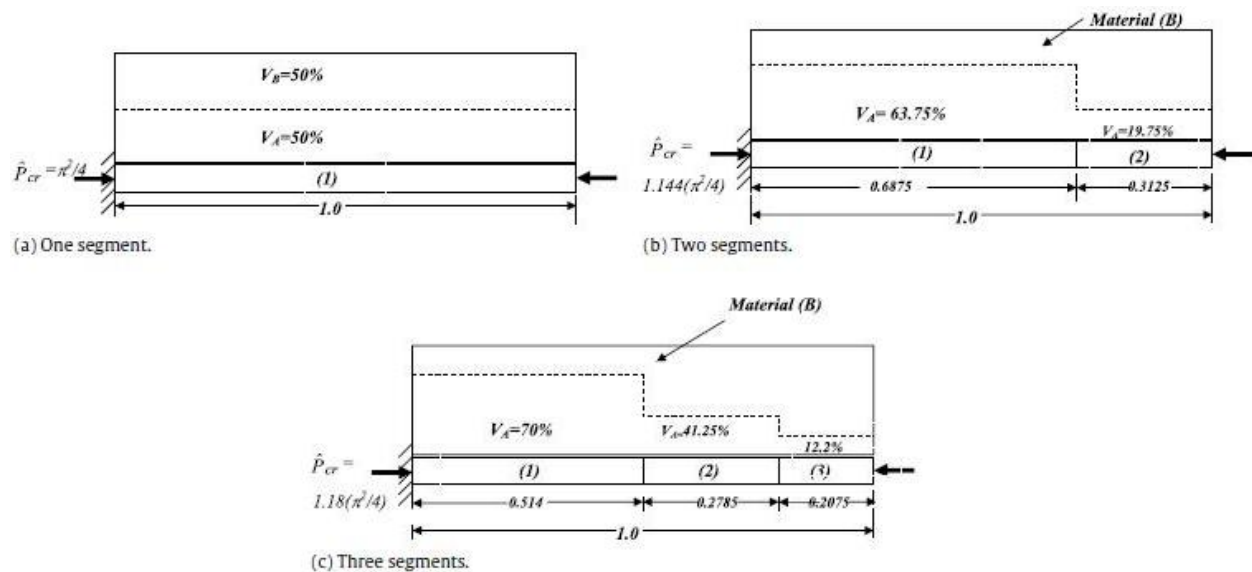


**Figure 6.** Strongest cantilevered columns with axial material grading: Material (A)=E-glass fibers, material (B)=epoxy matrix

### 3. Stability of FGM long cylinders under external pressure

A common application of composites is the design of cylindrical shells under the action of external hydrostatic pressure, which might cause collapse by buckling instability. Examples are the underground and underwater pipelines, rocket motor casing, boiler tubes subjected to external steam pressure, and reinforced submarine structures. The composite cylindrical vessels for underwater applications are intended to operate at high external hydrostatic pressure (sometimes up to 60 MPa). For deep- submersible long-unstiffened vessels, the hulls are generally realized using multilayered, cross-ply, composite cylinders obtained following the filament winding process. Previous numerical and experimental studies have shown that failure due to structural buckling is a major risk factor for thin laminated cylindrical shells. Figure 7 shows the structural model used in reference [13], where the effect of changing the fiber volume fraction in each lamina was taken in the formulation of the structural model.

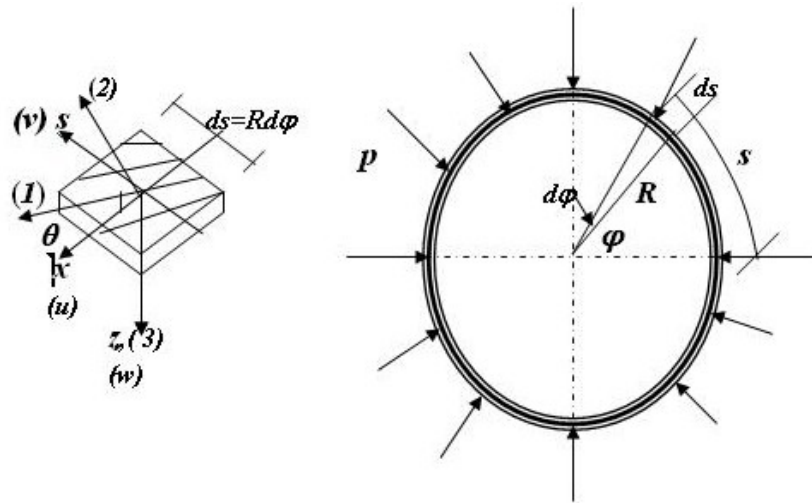


**Figure 7.** Laminated composite shell under external pressure ( $u$  displacement in the axial direction  $x$ ,  $v$  in the tangential direction  $s$ ,  $w$  in the radial direction  $z$ )

The governing differential equations of anisotropic rings/long cylinders subjected to external pressure are cast in the following [13]:

$$M'_{ss} + R(N'_{ss} - \beta N_{ss}) = \beta p R^2$$

$$M''_{ss} - R[N_{ss} + (\beta N_{ss})' + p(w_o + v'_o)] = p R^2 \quad (6)$$

where the prime denotes differentiation with respect to angular position  $\varphi$ , and  $\beta = (v_o - w'_o) / R$ . Two possible solutions for Eq. (6) can be obtained; one for the pre-buckled state and the other termed as the bifurcation solution obtained by perturbing the displacements about the pre-buckling solution. For laminated composite rings and long cylindrical shells the only significant strain components are the hoop strain ( $\epsilon_{ss}^o$ ) and the circumferential curvature ( $\kappa_{ss}$ ) of the mid-surface. In the case of thin rings the axial and

shear forces ( $N_{xx}$ ,  $N_{xs}$ ) must vanish along the free edges. The bending and twisting moments ( $M_{xx}$ ,  $M_{xs}$ ) may also be neglected. The final closed form solution for the critical buckling pressure is given by the following mathematical expression:

$$p_{cr} = 3 \left[ \frac{D_{ani}}{R^3} \right] \left[ \frac{1 - (\psi^2 / \alpha)}{1 + \alpha + 2\psi} \right], \quad \psi = \left( \frac{1}{R} \right) \left( \frac{B_{ani}}{A_{ani}} \right), \quad \alpha = \left( \frac{1}{R^2} \right) \left( \frac{D_{ani}}{A_{ani}} \right) \quad (7)$$

which is only valid for thin rings/cylinders with thickness-to-radius ratio  $(h/R) \leq 0.1$ . The stiffness coefficients  $A_{ani}$ ,  $B_{ani}$  and  $D_{ani}$  are calculated, for the case of long cylinders from:

$$\begin{bmatrix} A_{ani} & B_{ani} \\ B_{ani} & D_{ani} \end{bmatrix}_{cylinder} = \begin{bmatrix} A_{22} & B_{22} \\ B_{22} & D_{22} \end{bmatrix} \quad (8)$$

And for circular rings:

$$\begin{bmatrix} A_{ani} & B_{ani} \\ B_{ani} & D_{ani} \end{bmatrix}_{ring} = \begin{bmatrix} A_{22} & B_{22} \\ B_{22} & D_{22} \end{bmatrix} - [S_2]^T [S_1]^{-1} [S_2] \quad (9)$$

where

$$[S_1] = \begin{bmatrix} A_{11} & A_{16} & B_{11} & B_{16} \\ A_{16} & A_{66} & B_{16} & B_{66} \\ B_{11} & B_{16} & D_{11} & D_{16} \\ B_{16} & B_{66} & D_{16} & D_{66} \end{bmatrix} \quad \text{and} \quad [S_2] = \begin{bmatrix} A_{12} & B_{12} \\ A_{26} & B_{26} \\ B_{12} & D_{12} \\ B_{26} & D_{26} \end{bmatrix} \quad (10)$$

$A_{ij}$  are called the extensional stiffnesses given by:

$$A_{ij} = h \sum_{k=1}^n (\bar{Q}_{ij})_k (\hat{z}_k - \hat{z}_{k-1}) \quad (11)$$

$B_{ij}$  are called the bending-extensional stiffnesses given by:

$$B_{ij} = \frac{h^2}{2} \sum_{k=1}^n (\bar{Q}_{ij})_k (\hat{z}_k^2 - \hat{z}_{k-1}^2) \quad (12)$$

$D_{ij}$  are called the bending stiffnesses:

$$D_{ij} = \frac{h^3}{3} \sum_{k=1}^n (\bar{Q}_{ij})_k (\hat{z}_k^3 - \hat{z}_{k-1}^3) \quad (13)$$

where  $\hat{z}_k = z_k / h$  is a dimensionless coordinate, and  $\hat{h}_k = \hat{z}_k - \hat{z}_{k-1}$  is the dimensionless thickness of the  $k$ th lamina. The associated optimization problem shall seek maximization of the critical buckling pressure  $p_{cr}$  while maintaining the total structural mass constant at a value equals to that of a reference baseline design. Optimization variables include the fiber volume fraction ( $V_{fk}$ ), thickness ( $h_k$ ) and fiber orientation angle ( $\theta_k$ ) of the individual  $k$ -th ply,

$k=1, 2, \dots, n$  (total number of plies). Side constraints are always imposed on the design variables for geometrical, manufacturing or logical reasons to avoid having unrealistic odd shaped optimum designs. The first case study to be examined herein is a long thin-walled cylindrical shell fabricated from E-glass/epoxy composites with the lay-up made of only two plies ( $n=2$ ) having fibers parallel to the x-axis (i.e.  $\theta_1=\theta_2=0$ ). Considering the case with no side inequality constraints imposed on the design variables, Figure 8 shows the developed  $\hat{P}_{cr}$  - level curves, augmented with the mass equality constraint, in  $(V_{f1}-\hat{h}_1)$  design space.

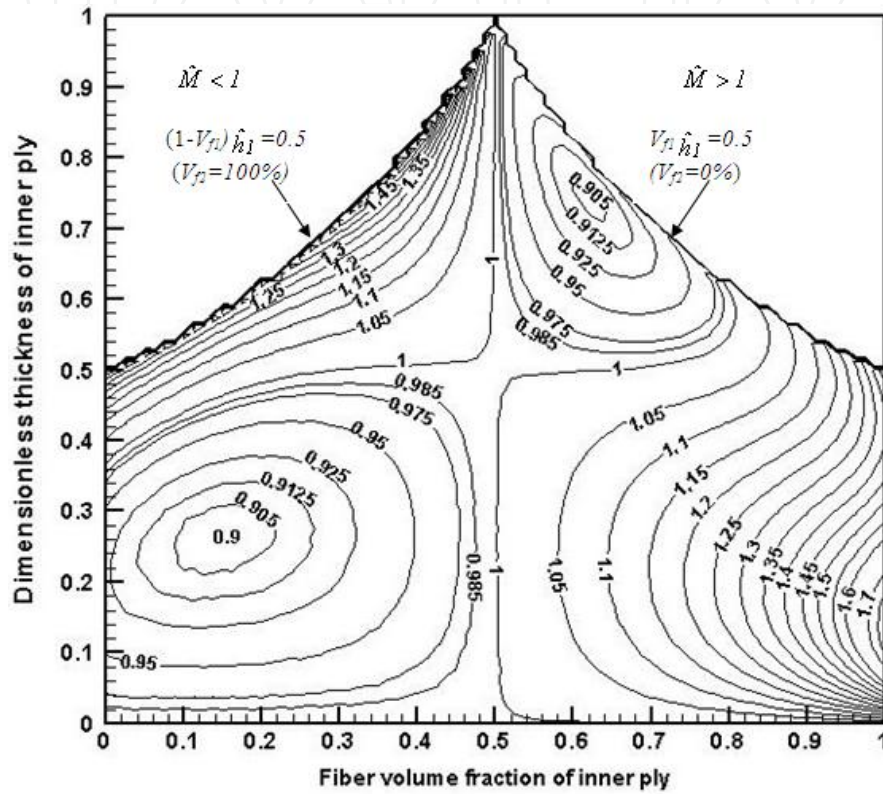
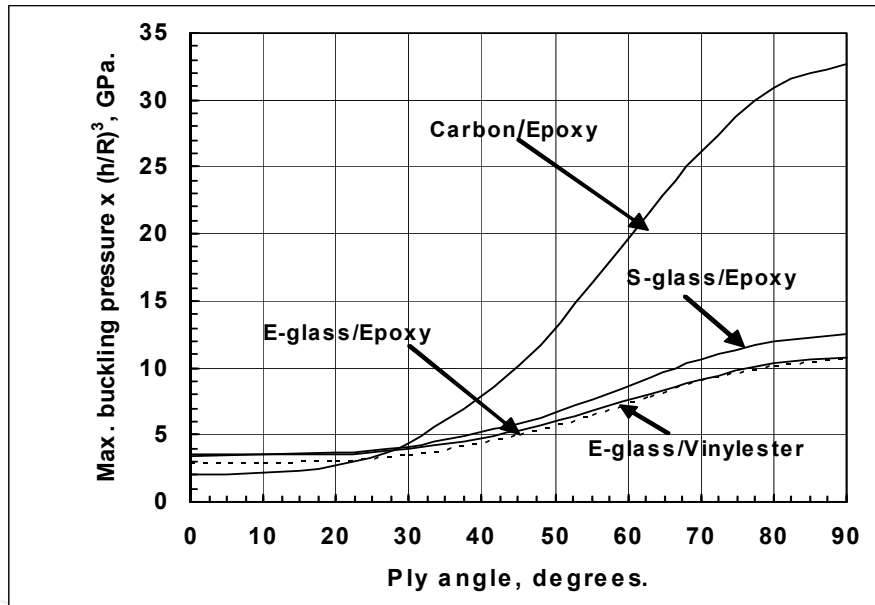


**Figure 8.** Optimum design space containing  $p_{cr}$ -isobars augmented with the mass equality constraint  $\hat{M} = 1.0$ . Case of two-layer, E-glass/epoxy cylinder with fibers parallel to cylinder axis ( $\theta_1=\theta_2=0$ ).

It is seen that such a constrained objective function is well behaved in the selected design space having the shape of a tent with its ceiling formed by two curved lines, above which the mass equality constraint is violated. Their zigzagged pattern is due to the obliged turning of many contours, which are not allowed to penetrate the tent's ceiling and violate the mass equality constraint. The curve to the left represent a 100% fiber volume fraction of the outer ply,  $V_{f2}$ , while the other curve to the right represents zero volume fraction, that is  $V_{f2}=0\%$ . Two local minima with  $p_{cr}$  near a value of 0.90 can be observed: one to the lower left zone near the design point  $(V_{fk}, h_k)_{k=1,2} = (0.15, 0.25), (0.6165, 0.75)$  while the other lies at the upper right zone close to the point  $(0.625, 0.745), (0.135, 0.255)$ . This represents degradation in the stability level by about 10.6% below the baseline value. On the other hand, the unconstrained absolute optimum value of the dimensionless critical buckling pressure was found to be 1.7874 at the design point  $(1.0, 0.145), (0.415, 0.855)$ . A more realistic optimum design has been obtained by imposing the side constraints:  $0.25 \leq V_{fk} \leq 0.75, k=1, 2$ . The

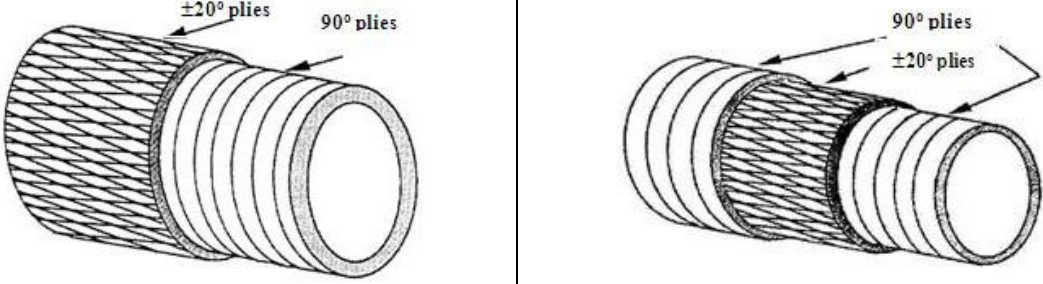


attained solution is  $(p_{cr})_{max} = 1.2105$  at the design point  $(0.75, 0.215)$ ,  $(0.4315, 0.785)$ , showing that good shell designs with higher stability level ought to have a thinner inner layer with higher fiber volume fraction and a thicker outer layer with less volume fraction. To see the effect of the ply angle, another case of study has been considered for a cylinder constructed from two balanced plies  $(\pm \theta)$  with equal thicknesses and same material properties of E-glass/epoxy composites. This type of stacking sequence is widely used in filament wound circular shells since such a manufacturing process inherently dictates adjacent  $(\pm \theta)$  layers. A local minimum was found near the design point  $(V_{fl}, \theta) = (0.375, 0.0)$  with  $p_{cr} = 0.9985$ , indicating a degradation in the stability level below the baseline design. The absolute maximum occurred at the design points  $(V_{fl}, \theta) = (0.5, \pm 90^\circ)$  with  $(p_{cr})_{max} = 3.45766$ , which means that the dimensional critical pressure,  $p_{cr} = 3.45766 \times 2.865 = 9.906 \times (h/R)^3$  GPa. Figure 9 depicts the final global optimum designs of cylinders constructed from adjacent  $(+ \theta)$  and  $(- \theta)$  plies for the different types of the selected composite materials. All shall have the same optimal solution  $(V_{fk}, h_k)_{k=1,2} = (0.75, 0.215)$ ,  $(0.4315, 0.785)$ , independent upon the shell thickness-to-radius ratio  $(h/R)$ , a major contribution of the given formulation.



**Figure 9.** Variation of the absolute maximum buckling pressure with ply angle for balanced  $(\pm \theta)$  cylinders with structural mass preserved constant

Other cases of study include optimization of two different constructions of multi-layered cylinders made of AS-4 carbon/epoxy composites. The first one is called a lumped-layup construction with the inner half of its wall composed of  $90^\circ$  hoop layers and the outer half made of  $\pm 20^\circ$  helically wound layers. The second type has different stacking sequence where the  $\pm 20^\circ$  layers are sandwiched in between outer and inner  $90^\circ$  hoop layers. Optimum solutions are given in Table 4, indicating that good designs shall have thicker hoop wound layers with higher volume fraction of the fibers near the upper limiting values imposed by the manufacturers. On the other hand, the sandwiched helically wound layers are seen to be thinner and have less fiber volume fractions.

$(h/R)$	[90°/±20°] layup		[90°/±20°/90°] layup	
	$p_{cr,max}=9.37 \times (10h/R)^3$ MPa		$p_{cr,max}=36.634 \times (10h/R)^3$ MPa	
	Optimum value	% gain	Optimum value	% gain
1/50	0.075	17.19	0.293	26.84
1/25	0.596	15.5	2.344	26.84
1/20	1.171	15.6	4.579	26.91
1/15	2.776	14.81	10.854	26.92
				
<b>Optimum solutions</b>				
<b>Two helical layers</b> ( $V_f, h, \theta$ )=	(0.25, 0.225, ±20°)		(0.2925, 0.235, ±20°)	
<b>Two hoop layers</b> ( $V_f, h, \theta$ )=	(0.705, 0.275, 90°)		(0.6835, 0.265, 90°)	

**Table 4.** Optimum buckling design of multi-layered, AS-4, FGM composite cylinders

#### 4. Dynamic optimization of FGM bars in axial motion

Elastic slender bars in axial motion can give rise to significant vibration problems, which assesses the importance of considering optimization of natural frequencies. These frequencies, besides being maximized, must be kept out of the range of the excitation frequencies in order to avoid large induced stresses that can exceed the reserved fatigue strength of the materials and, consequently, cause failure in a short time. Expressed mathematically, two different design criteria are implemented here for optimizing frequencies:

**Frequency-placement criterion:** Minimize  $\sum_i W_{fi} \omega_i$  (14)

**Maximum-frequency criterion:** Maximize  $\sum_i W_{fi} \omega_i$  (15)

In both criteria, an equality constraint should be imposed on the total structural mass in order not to violate other economic and performance requirements. Equation (10) represents a weighted sum of the squares of the differences between each important frequency  $\omega_i$  and its



desired (target) frequency  $\omega_i^*$ . Appropriate values of the target frequencies are usually chosen to be within close ranges (called frequency windows) of those corresponding to a reference or baseline design, which are adjusted to be far away from the critical exciting frequencies. The main idea is to tailor the mass and stiffness distributions in such a way to make the objective function a minimum under the imposed mass constraint. The second alternative for reducing vibration is the direct maximization of the system natural frequencies as expressed by equation (11). Maximization of the natural frequencies can ensure a simultaneous balanced improvement in both of stiffness and mass of the vibrating structure. It is a much better design criterion than minimization of the mass alone or maximization of the stiffness alone. The latter can result in optimum solutions that are strongly dependent on the limits imposed on either the upper values of the allowable deflections or the acceptable values of the total structural mass, which are rather arbitrarily chosen. The proper determination of the weighting factors  $W_{fi}$  should be based on the fact that each frequency ought to be maximized from its initial value corresponding to a baseline design having uniform mass and stiffness properties. Reference [14] applied the concept of material grading for enhancing the dynamic performance of bars in axial motion. The associated eigenvalue problem is cast in the following:

$$\hat{E} \frac{d^2 \hat{U}}{d\hat{x}^2} + \frac{d\hat{E}}{d\hat{x}} \cdot \frac{d\hat{U}}{d\hat{x}} + \hat{\rho} \hat{\omega}^2 \hat{U} = 0, \quad 0 < \hat{x} < 1 \quad (16)$$

where  $\hat{U} = U/L$  is the dimensionless amplitude and  $\hat{\omega} = \omega L \sqrt{\rho/E}$  dimensionless frequency. Both continuous and discrete distributions of the volume fractions of the selected composite material were analyzed in [14]. The general solution of Eq. (12), where the modulus of elasticity and mass density vary in the axial direction, can be expressed by the following power series:

$$\hat{U}(\hat{x}) = \sum_{m=1}^2 C_m \lambda_m(\hat{x}) \quad (17)$$

where  $C_m$ 's are the constants of integration and  $\lambda_m$ 's are two linearly independent solutions that have the form:

$$\lambda_m(\hat{x}) = \sum_{n=m}^{\infty} a_{m,n} \hat{x}^{n-1} \quad (n \geq m) \quad (18)$$

The unknown coefficients  $a_{m,n}$  can be determined by substitution into the differential equation (12) and equating coefficients of like powers of  $\hat{x}$ . Table 5 summarizes the appropriate mathematical expressions of the frequency equation for any desired case, which can be obtained by application of the associated boundary conditions and consideration of nontrivial solutions.

Variation of the volume fractions in FGM structures is usually described by power-law distributions. Figure 10 shows both linear and parabolic models for material grading along the bar span. Results given in [14] showed that, for Fixed-Fixed and Fixed-Free boundary conditions, patterns with higher fiber volume fraction near the fixed ends are always

	Boundary conditions	Frequency equation	$(\hat{\omega}_o)_i$
Fixed-Fixed Bar Symmetrical modes Unsymmetrical modes	$\hat{U}(0) = \hat{U}'(1/2) = 0$	$\sum_{n=3}^{\infty} a_{2n}(n-1)/(2)^{n-2} = -1$	$(\pi, 3\pi, 5\pi)$
	$\hat{U}(0) = \hat{U}(1/2) = 0$	$\sum_{n=2}^{\infty} a_{2n}/(2)^{n-1} = 0$	$(2\pi, 4\pi, 6\pi)$
Fixed-Free Bar	$\hat{U}(0) = \hat{U}'(1) = 0$	$\sum_{n=3}^{\infty} a_{2n}(n-1) = -1$	$(\pi, 3\pi, 5\pi)/2$
Free-Free Bar Symmetrical modes Unsymmetrical modes	$\hat{U}'(0) = \hat{U}'(1/2) = 0$	$\sum_{n=3}^{\infty} a_{1n}(n-1)/(2)^{n-2} = 0$	$(2\pi, 4\pi, 6\pi)$
	$\hat{U}'(0) = \hat{U}(1/2) = 0$	$\sum_{n=3}^{\infty} a_{1n}/(2)^{n-1} = -1$	$(\pi, 3\pi, 5\pi)$

**Table 5.** Frequency equations for different types of boundary conditions.  $\hat{\omega}_{o,i}$  are the dimensionless natural frequencies of the baseline design ( $\hat{\omega}_o=0$  corresponding to the first rigid body mode of a Free-Free bar). The notation  $(\hat{\omega}_o)'$  means  $d/d\hat{x}$ .

favorable. The opposite trend is true for cases of Free-Free bars. Maximization of the fundamental frequency alone produces an optimization gain of about 14.33% for the linear model with 0% and 100% volume fractions at the ends of the optimized bars with different boundary conditions. However, a drastic reduction in the 2<sup>nd</sup> and 3<sup>rd</sup> frequencies was observed. Better solutions have been achieved by maximizing a weighted-sum of the first three frequencies, where the parabolic model was found to excel the linear one in producing balanced improvements in all frequencies. Results have also indicated that the Fixed-Fixed bars are recommended to have concave distribution rather than convex one. The latter produce poor patterns with degraded stiffness-to-mass ratio levels. The opposite trend was observed for the free-free bars, where the convex type is much more favorable than the concave type. Both concave and convex shapes can be accepted for a cantilevered bar. For piecewise models, the developed isomerits for the case of Free-Free bar built of four symmetrical segments made of carbon/epoxy composites are shown in Figure 11. The global maximum of the fundamental frequency is located at the lower region to the left of the design space having a value of  $\hat{\omega}_{1,max} = 3.45406$  at the optimal design point  $(V_A, \hat{L})_{k=1,2} = (0.1885, 0.1625), (0.650, 0.3375)$ , which represents about 10% optimization gain.

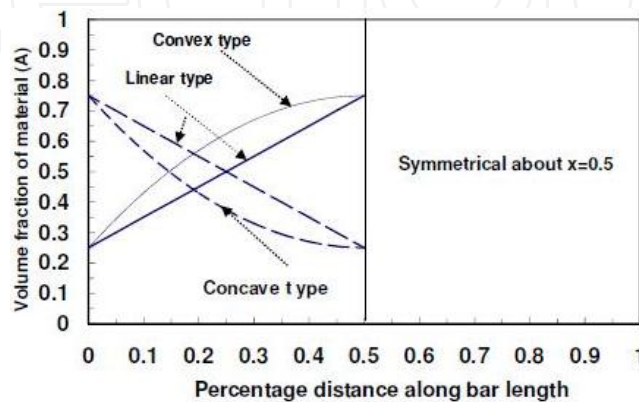
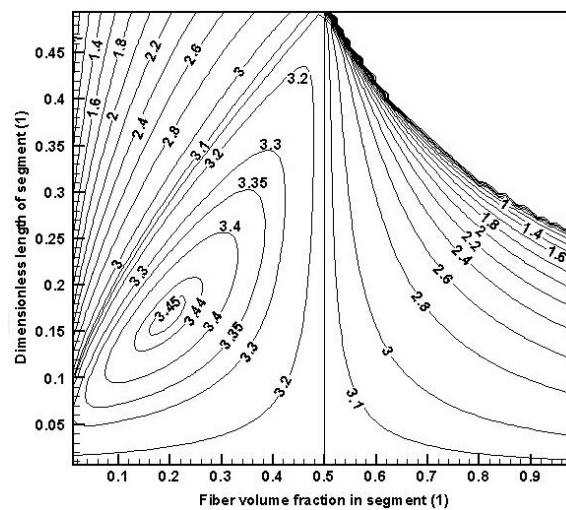
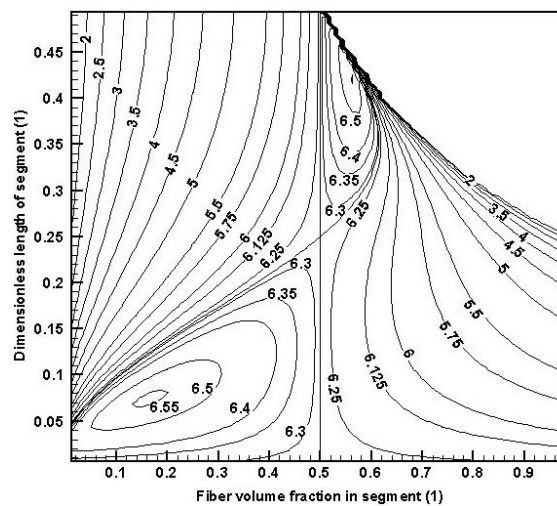


**Figure 10.** Symmetrical shape models of volume fraction distribution along bar length



(a) Fundamental frequency (Unsymmetrical mode)



(b) Second frequency (Symmetrical mode).

**Figure 11.** Dimensionless frequency isomerits of free-free bar under mass constraint

## 5. Material grading for improved aeroelastic stability of composite wings

Aircraft wings can experience aeroelastic instability condition in high speed flight regimes. A solution that can be promising to enhance aeroelastic stability of composite wings is the use of the concept of functionally graded materials (FGMs) with spatially varying properties. Reference [15] introduced some of the underlying concepts of using material grading in optimizing subsonic wings against torsional instability. Exact mathematical approach allowing the material properties to change in the wing spanwise direction was applied, where both continuous and piecewise structural models were successfully implemented. The enhancement of the torsional stability was measured by maximization of the critical flight speed at which divergence occurs with the total structural mass kept at a

constant value in order not to violate other performance requirements. Figure 12 shows a rectangular composite wing model constructed from uniform piecewise panels, where the design variables are defined to be the fiber volume fraction ( $V_f$ ) and length ( $L$ ) of each panel.

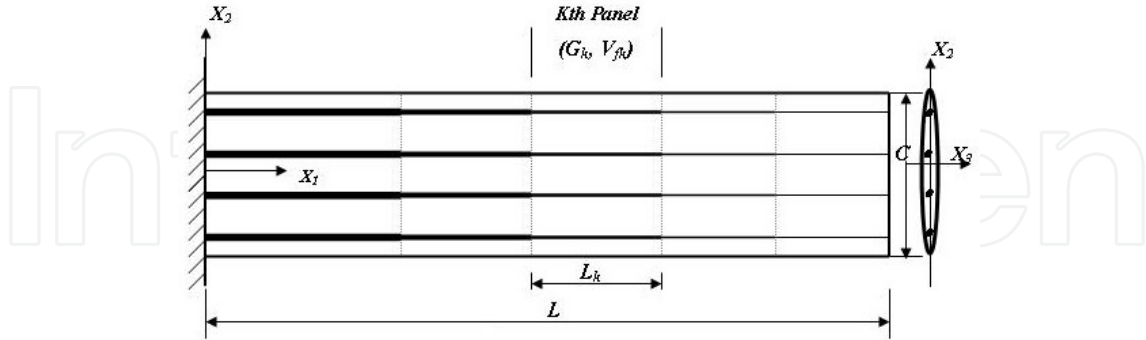


**Figure 12.** Composite wing model with material grading in spanwise direction

The isodiverts (lines of constant divergence speed) for a wing composed from two panels made of carbon-AS4/epoxy-3501-6 composite are shown in Figure 13. The selected design variables are  $(V_{f1}, L_1)$  and  $(V_{f2}, L_2)$ . However, one of the panel lengths can be eliminated, because of the equality constraint imposed on the wing span. Another variable can also be discarded by applying the mass equality constraint, which further reduces the number of variables to only any two of the whole set of variables. Actually the depicted level curves represent the dimensionless critical flight speed augmented with the imposed equality mass constraint. It is seen that the function is well behaved, except in the empty regions of the first and third quadrants, where the equality mass constraint is violated. The final constrained optima was found to be  $(V_{f1}, L_1) = (0.75, 0.5)$  and  $(V_{f2}, L_2) = (0.25, 0.5)$ , which corresponds to the maximum critical speed of 1.81, representing an optimization gain of about 15% above the reference value  $\pi/2$ . The functional behavior of the critical flight speed  $\hat{V}_{div}$  of a three-panel model is shown in Figure 14, indicating conspicuous design trends for configurations with improved aeroelastic performance. As seen, the developed isodiverts have a pyramidal shape with its vertex at the design point  $(V_{f2}, L_2) = (0.5, 1.0)$  having  $\hat{V}_{div} = \pi/2$ . The feasible domain is bounded from above by the two lines representing cases of two-panel wing, with  $V_{f1} = 0.75$  for the line to the left and  $V_{f3} = 0.25$  for the right line. The contours near these two lines are asymptotical to them in order not to violate the mass equality constraint. The final global optimal solution, lying in the bottom of the pyramid, was calculated using the MATLAB optimization toolbox routines as follows:  $(V_{fk}, L_k)_{k=1,2,3} = (0.75, 0.43125), (0.5, 0.1375), (0.25, 0.43125)$  with  $\hat{V}_{div} = 1.82$ , which represents an optimization gain of about 16%. Actually, the given exact mathematical approach ensured the attainment of global optimality of the proposed optimization model. A more general case would include material grading in both spanwise and airfoil thickness directions.

## 6. Optimization of FGM pipes conveying fluid

The determination of the critical flow velocity at which static or dynamic instability can be encountered is an important consideration in the design of slender pipelines containing

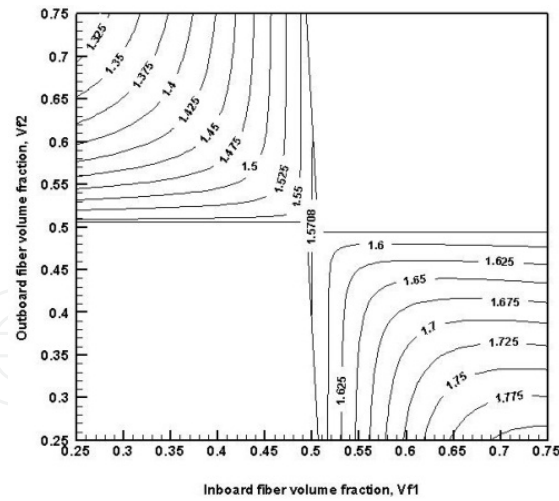


**Figure 13.** Isodiverts of for a two-panel wing model

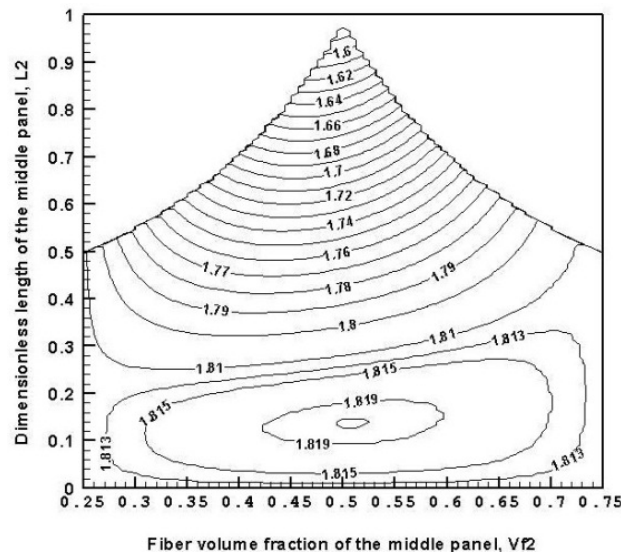


**Figure 14.** Isodiverts of  $\hat{V}_{div}$  in  $(V_{L2}-L2)$  design space for a three-panel wing model

flowing fluid. At sufficiently high flow velocities, the transverse displacement can be too high so that the pipe bends beyond its ultimate strength leading to catastrophic instabilities. In fact maximization of the critical flow velocity can be regarded as a major aspect in designing an efficient piping system with enhanced flexural stability. It can also have other desirable effects on the overall structural design and helps in avoiding the occurrence of large displacements, distortions and excessive vibrations, and may also reduce fretting among structural parts, which is a major cause of fatigue failure. The dynamic characteristics of fluid-conveying functionally graded materials cylindrical shells were investigated in [16]. A power-law was implemented to model the grading of material properties across the shell thickness and the analysis was performed using modal superposition and Newmark's direct time integration method. Reference [17] presented an analytical approach for maximizing the critical flow velocity, also known as divergence velocity, through multi-module pipelines for a specified total mass. Optimum solutions



were given for simply supported pipes with the design variables taken to be the wall thickness and length of each module composing the pipeline. A recent work [18] considered stability optimization of FGM pipelines conveying fluid, where a general multimodal model was formulated and applied to cases with different boundary conditions. A more spacious optimization model was given and extending the analysis to cover both effects of material, thickness grading and type of support boundary conditions. The model incorporated the effect of changing the volume fractions of the constituent materials for maximizing the critical flow velocity while maintaining the total mass at a constant value. Additional constraints were added to the optimization model by imposing upper limits on the fundamental eigenvalue to overcome the produced multiplicity near the optimum solution. Figure 15 shows the pipe model under consideration consisting of rigidly connected thin-walled tubes, each of which has different material properties, cross-sectional dimensions and length. The tube thickness,  $h$ , is assumed to be very small as compared with the mean diameter,  $D$ . The pipe conveys an incompressible fluid flowing steadily with an axial velocity  $U_k$  through the  $k$ th module. The variation in the velocity across the cross section was neglected, and the pipe was assumed to be long and slender so that the classical engineering theory of bending can be applicable. The effects of structural damping, damping of surroundings and gravity were not considered. Practical designs ignoring small damping, which has stabilizing effect on the system motion, are always conservatives. The model axis in its un-deformed state coincides with the horizontal  $x$ -axis, and the free small motion of the pipe takes place in a two dimensional plane with transverse displacement,  $w$ .

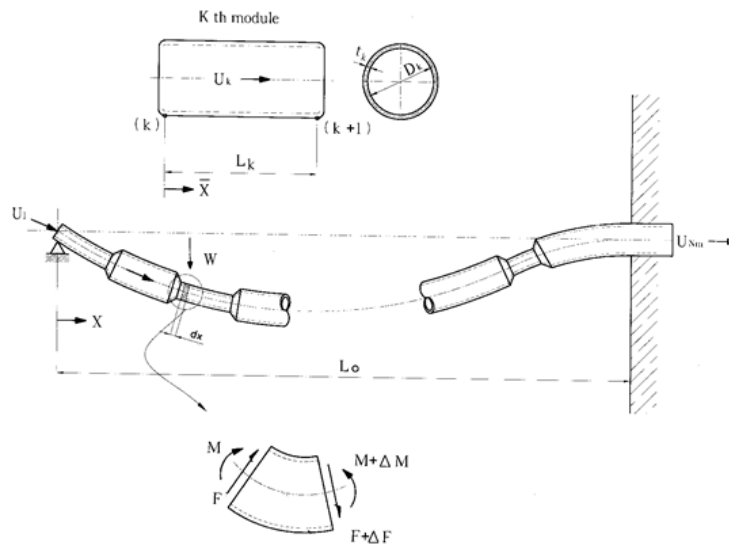


**Figure 15.** General configuration of a piecewise axially graded pipe conveying fluid.

The various parameters are normalized by their corresponding values of a baseline pipe having the same total mass and length, material and fluid properties, and boundary conditions as well. The baseline pipe has uniform mass and stiffness distributions along its length and is made of two different materials denoted by (A) and (B) with equal volume fractions ( $V$ ), i.e.  $V_A = V_B = 50\%$ . The governing differential equation in dimensionless form:

$$w'''' + \lambda_k^2 w'' = 0 \quad (19)$$

$$\text{where } \lambda_k = U_k \sqrt{\frac{A_k}{E_k I_k}} = \frac{U A_{max}}{\sqrt{A_k E_k I_k}}$$

$$k=1,2,\dots,N_m \quad (20)$$

which is valid over the length of any  $k$ th module of the pipe, i.e.  $0 \leq \bar{x} \leq L_k$ , where  $\bar{x} = x - x_k$

In equation (16),  $U$  stands for the flow velocity through the pipe module having the maximum cross sectional area  $A_{max}$  and  $N_m$  is the total number of modules composing the pipeline. It is noted that consideration of the continuity equation provides that  $U_k A_k = U A_{max}$ ,  $k=1,2,\dots,N_m$ . Possible boundary conditions at the end supports of the pipeline are stated in the following:

- (a) Hinged-Hinged (H/H):  $w(0)=w''(0)=0$   
 $w(1)=w''(1)=0$
- (b) Clamped-Hinged (C/H):  $w(0)=w''(0)=0$   
 $w(1)=w'(1)=0$
- (c) Clamped-Clamped (C/C):  $w(0)=w'(0)=0$   
 $w(1)=w'(1)=0$

For a cantilevered pipeline, static instability caused by divergence is unlikely to happen. The non-trivial solution of the associated characteristic equation results in a vanishing bending displacement over the entire span of the pipeline. For such pipe configuration, dynamic instability (flutter) may only be considered. The state variable are defined by the vector

$$\underline{Z}_k^T = [w \ \phi \ M \ F]_k = [w - w' - EIw'' - EIw''']_k \quad (21)$$

At two successive joints ( $k$ ) and ( $k+1$ ) the state vectors are related to each other by the matrix equation

$$\underline{Z}_{k+1} = [T_k] \underline{Z}_k \quad (22)$$

where  $[T_k]$  is a square matrix of order  $4 \times 4$  known as the transmission or transfer matrix of the  $k$ th pipe module. For a pipeline built from  $N_m$  - uniform modules, Eq.(18) can be applied at successive joints to obtain

$$\underline{Z}_{Nm+1} = [T] \underline{Z}_1 \quad (23)$$

where  $[T]$  is called the overall transmission matrix formed by taking the products of all the intermediate matrices of the individual modules. Therefore, applying the boundary conditions and considering only the non-trivial solution, the resulting characteristic equation can be solved numerically for the critical flow velocity,  $U$ . Extensive computer experimentation for obtaining the non-trivial solution of Eq.(19), for various pipe configurations, has demonstrated that the critical velocity can be multiple in some zones in the design space. This means that the eigenvalues cross each other, indicating multi-modal



solutions (i.e. Bi- Tri- Quadri- modal solutions). Such a multiplicity introduces singularity of the eigenvalue derivatives with respect to the design variables, which does not allow the use of gradient methods. Therefore, it is necessary to formulate the optimization problem with respect to the critical velocity connected with two, three, or four simultaneous divergence modes. The present formulation employs multi-dimensional, non-gradient search techniques to find the required optimum solutions [2, 3]. This formulation requires only simple function evaluations without computing any derivatives for either the objective function or the design constraints. The additional constraints, which ought to be added to the optimization problem, are [18]:

$$U_1 \leq U_j, \quad j=2,3,\dots,m. \quad (24)$$

where  $U_1$  is the first eigenvalue representing the dimensionless critical flow velocity,  $U_j$ 's are the subsequent higher eigenvalues and  $m$  is the assumed modality of the final optimum solution. All constraints are augmented with the objective function through penalty multiplier terms, and the number of active constraints at the optimum design point can automatically detect the actual modality of the problem. In the case of single mode optimization, none of the constraints become active at the optimal solution. It is noted that the total mass and length equality constraints can be used to eliminate some of the design variables, which help reducing the dimensionality of the optimization problem. The *MATLAB* optimization toolbox is a powerful tool that includes many routines for different types of optimization encompassing both unconstrained and constrained minimization algorithms [3]. One of its useful routines is named "*fmincon*" which finds the constrained minimum of an objective function of several variables. Figure 16 depicts the functional behavior of the dimensionless critical flow velocity,  $U_{cr,1}$  augmented with the equality mass constraint,  $M_s=1$ . It is seen that the function is well behaved and continuous everywhere in the design space  $(V_f, L)_1$ , except in the empty region located at the upper right of the whole domain, where the mass equality constraint is violated. The feasible domain is seen to be split by the baseline contours ( $U_{cr}=\pi$ ) into two distinct zones. The one to the right encompasses the constrained global maxima, which is calculated to be  $U_{cr}=3.2235$  at the optimal design point  $(V_f, L)_{k=1,2}=(0.550, 0.80), (0.30, 0.20)$ . Actually, each design point inside the feasible domain corresponds to different material properties as well as different stiffness and mass distributions, while maintaining the total structural mass constant. Figure 17 shows the developed isodiverts (lines of constant divergence velocity,  $U_{cr,1}$ ) in the  $(V_{f1}-V_{f2})$  design space. The equality mass constraint is violated in the first and third quadrants and the cross lines  $V_{f1}=50\%$  and  $V_{f2}=50\%$  represent the isodiverts of the baseline value  $\pi$ . For the case of a clamped-hinged (C/H), two-module pipe, the global maxima was calculated to be  $(V_f, L)_{k=1,2}=(0.525, 0.875), (0.325, 0.125)$  at which  $U_{cr,1}=4.5645$ . Table 6 summarizes the attained optimal solutions for the different types of boundary conditions. Cases of combined material and thickness grading are also included, showing a truly and significant optimization gain for the different pipe configurations. More results indicated that for the case of H/H pipelines, good patterns must be symmetrical about the mid-span point. Therefore, it can be easier to cope with symmetrical configurations, which reduce computational efforts significantly, and the total number of variables to half. In this case, the boundary conditions

become  $w(0)=w'(0)=0$  and  $w(1/2)=w'(1/2)=0$ . For three-module  $H/H$  pipeline, the attained maximum value of the critical velocity was found to be 3.7955, occurring at the design point  $(V_f, h, L)_k = (0.625, 0.5, 0.15625), (0.7, 1.1375, 0.6875), (0.625, 0.5, 0.15625)$ . This represents about 20.81% optimization gain above the baseline value  $\pi$ .

Support	$(V_f, h, L)_{k=1,2}$	$U_{cr,max}$
<b>Material grading only</b>		
H/H	$(0.550, 1.0, 0.800), (0.300, 1.0, 0.200)$	3.2235
C/H	$(0.525, 1.0, 0.875), (0.325, 1.0, 0.125)$	4.5645
C/C	$(0.675, 1.0, 0.125), (0.475, 1.0, 0.875)$	6.3325
<b>Combined material &amp; thickness grading</b>		
H/H	$(0.70, 1.0, 0.75), (0.65, 0.75, 0.25)$	3.6235
C/H	$(0.70, 0.95, 0.9), (0.50, 0.85, 0.10)$	5.1355
C/C	$(0.70, 1.0, 0.60), (0.65, 0.85, 0.40)$	7.0965

**Table 6.** Optimal solutions for two-module pipelines

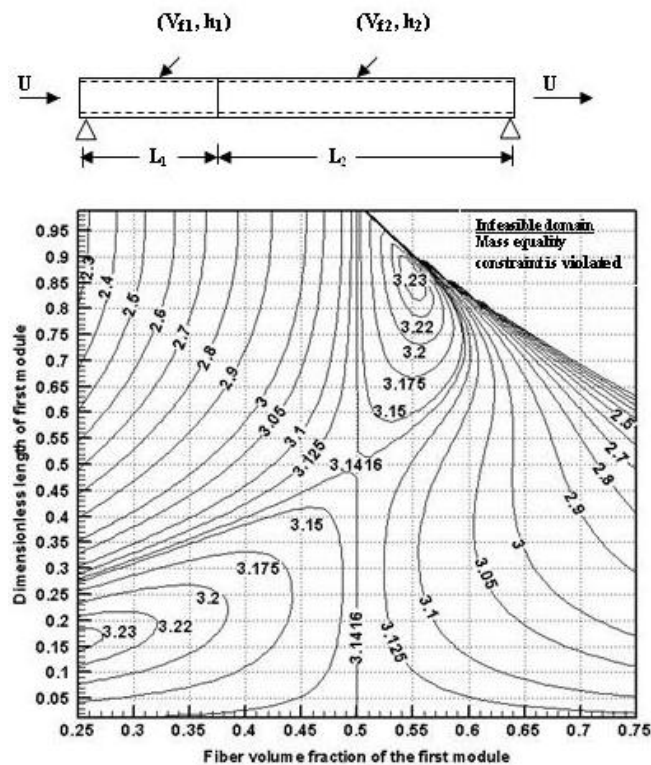


**Figure 16.** Effect of material grading on the critical flow velocity for a two-module,  $H/H$  pipe with constant total mass.

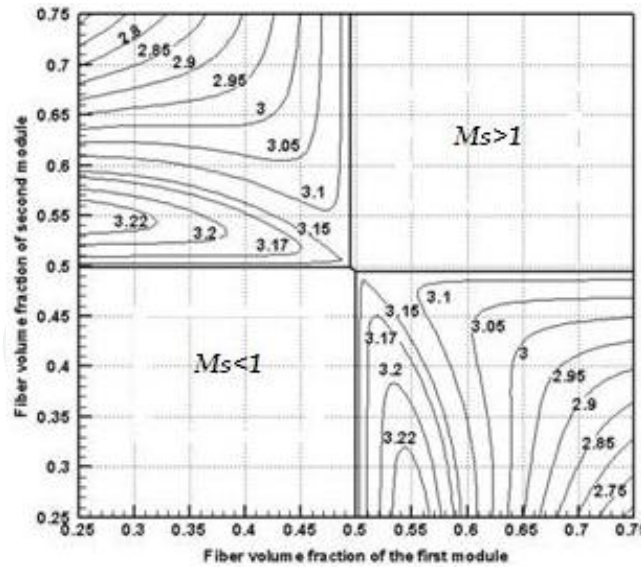


**Figure 17.** Isodiverts in the  $(V_1-V_2)$  design space for a two-module,  $H/H$  pipe.

## 7. Conclusion

As a major concern in producing efficient structures with enhanced properties and tailored response, this chapter presented appropriate design optimization models for improving performance and operational efficiency of different types of composite structural members. The concept of material grading was successfully applied by incorporating the distribution of the volume fractions of the composite material constituents in the mathematical formulation. Different optimization strategies have been addressed, including maximization of buckling stability of columns and cylindrical shells, natural frequencies of vibrating bars and critical flight speed of subsonic wings. Other stability problems concerning fluid-structure interaction has also been addressed. The general set of design variables encompasses volume fraction distribution, geometry and cross-sectional parameters. It has been shown that normalization of all quantities results in a naturally scaled objective functions, constraints and design variables, which is recommended when applying different optimization techniques. Piecewise models including multi-segment and multi-layered composite structures are implemented, where the optimized designs can be fabricated economically from any arbitrary number of uniform segments with material grading in a predetermined direction. Several design charts that are useful for direct determination of the optimal values of the design variables are given. It has been confirmed that the segment length is most significant design variable in the whole optimization process. Some investigators who apply finite elements have not recognized that the length of each element can be taken as a main design variable in the whole set of optimization variables. The results from the present approach reveal that piecewise grading of the material can be promising producing truly efficient designs with enhanced stability, dynamic and aeroelastic performance. Actually, the most economic structural design that will perform its intended function with adequate safety and durability requires much more than the procedures that have been described in this chapter. It is the author's wish that the results presented in this

chapter will be compared and validated through other optimization techniques such as genetic algorithms or any appropriate global optimization algorithm. Further optimization studies must depend on a more accurate analysis of constructional cost. This combined with probability studies of load applications and materials variations, should contribute to further efficiency achievement. Much improved and economical designs for the main structural components may be obtained by considering multi-disciplinary design optimization, which allows designers to incorporate all relevant design objectives simultaneously. Finally, it is important to mention that, while FGM may serve as an excellent optimization and material tailoring tool, the ability to incorporate optimization techniques and solutions in practical design depend on the capacity to manufacture these materials to required specifications. Conventional techniques are often incapable of adequately addressing this issue. In conclusion, FGMs represent a rapidly developing area of science and engineering with numerous practical applications. The research needs in this area are uniquely numerous and diverse, but FGMs promise significant potential benefits that fully justify the necessary effort.

## Author details

Karam Maalawi

*National Research Centre, Mechanical Engineering Department, Cairo, Egypt*

## 8. References

- [1] Maalawi K., Badr M. (2009) Design Optimization of Mechanical Elements and Structures: A Review with Application. *Journal of Applied Sciences Research* 5(2): 221–231.
- [2] Rao S. (2009) *Engineering Optimization: Theory and Practice*, 4<sup>th</sup> edition, John Wiley & Sons, ISBN: 978-0470183526, New York.
- [3] Venkataraman P. (2009) *Applied Optimization with MATLAB Programming*, 2<sup>nd</sup> edition, John Wiley & Sons, ISBN: 978-0470084885, New York.
- [4] Daniel I., Ishai O. (2006) *Engineering Mechanics of Composite Materials*, 2<sup>nd</sup> ed., Oxford Univ. Press, New York.
- [5] Birman V., Byrd W. (2007) Modeling and Analysis of Functionally Graded Materials and Structures. *Applied Mechanics Reviews*, ASME 60: 195-216.
- [6] Elishakoff I., Guede Z. (2004) Analytical Polynomial Solutions for Vibrating Axially Graded Beams. *Journal of Mechanics and Advanced Materials and Structures*, 11: 517-533.
- [7] Elishakoff I., Endres J. (2005) Extension of Euler's Problem to Axially Graded Columns: Two Hundred and Sixty Years Later. *Journal of Intelligent Material systems and Structures*, 16(1): 77-83.
- [8] Shi-Rong Li, Batra R. (2006) Buckling of Axially Compressed Thin Cylindrical Shells with Functionally Graded Middle Layer. *Journal of Thin-Walled Structures*, 44: 1039-1047.
- [9] Qian L., Batra R. (2005) Design of Bidirectional Functionally Graded Plate for Optimal Natural Frequencies. *Journal of Sound and Vibration*, 280: 415-424.

- [10] Goupee A., Vel S. (2006) Optimization of Natural Frequencies of Bidirectional Functionally Graded Beams. *Journal of Structural and Multidisciplinary Optimization*, 32(6): 473-484.
- [11] Maalawi K. (2002) Buckling Optimization of Flexible Columns. *International Journal of Solids and Structures*, 39: 5865-5876.
- [12] Maalawi K. (2009) Optimization of Elastic Columns using Axial Grading Concept. *Engineering Structures*, 31(12): 2922-2929.
- [13] Maalawi K. (2011) Use of Material Grading for Enhanced Buckling Design of Thin-Walled Composite Rings/Long Cylinders under External Pressure. *Composite Structures*, 93(2): 351-359.
- [14] Maalawi K. (2011) Functionally Graded Bars with Enhanced Dynamic Performance. *Journal of Mechanics of Materials and Structures*, 6(1-4): 377-393.
- [15] Librescu L., Maalawi K. (2007) Material Grading for Improved Aeroelastic Stability in Composite Wings. *Journal of Mechanics of Materials and Structures*, 2(7): 1381-1394.
- [16] Sheng G., Wang, X. (2010) Dynamic Characteristics of Fluid-Conveying Functionally Graded Cylindrical Shells under Mechanical and Thermal Loads. *Composite Structures*, 93(1): 162-170.
- [17] Maalawi, K. and Ziada, M. (2002). On the Static Instability of Flexible Pipes Conveying Fluid. *Journal of Fluids and Structures*, 16(5): 685-690.
- [18] Maalawi K., EL-Sayed H. (2011) Stability Optimization of Functionally Graded Pipes Conveying Fluid. *Proceedings of the International Conference of Mechanical Engineering, World Academy of Science, Engineering and Technology, Paris, France, July 27-29, 2011*, 178-183.